

## REFINEMENT OF THE KAOLINITE STRUCTURE FROM SINGLE-CRYSTAL SYNCHROTRON DATA

R. B. NEDER,<sup>1,†</sup> M. BURGHAMMER,<sup>1,‡</sup> TH. GRASL,<sup>1</sup> H. SCHULZ,<sup>1</sup> A. BRAM,<sup>2,§</sup> AND S. FIEDLER<sup>2</sup>

<sup>1</sup> Institut für Kristallographie, Theresienstr. 41, 80333 München, Germany

<sup>2</sup> ESRF, B.P. Box 220, 38043 Grenoble, France

**Abstract**—The crystal structure of single crystals of kaolinite from Keokuk, Iowa, was refined using data measured at the microfocus X-ray beamline at the ESRF, Grenoble, France ( $\lambda = 0.6883$ ,  $T = \text{room temperature}$ ). The volume of the crystals was 8 and  $0.8 \mu\text{m}^3$ , respectively. Unit-cell parameters are:  $a = 5.154(9) \text{ \AA}$ ,  $b = 8.942(4) \text{ \AA}$ ,  $c = 7.401(10) \text{ \AA}$ ,  $\alpha = 91.69(9)^\circ$ ,  $\beta = 104.61(5)^\circ$ ,  $\gamma = 89.82(4)^\circ$ . Space group  $C1$  is consistent with the observed data. All non-hydrogen atoms were independently refined with anisotropic displacement parameters. The positions and isotropic displacement parameters for the three interlayer H atoms were refined also. The position of the intralayer H was found by difference-Fourier methods, although refinement was not possible. Difference-Fourier maps suggested large anisotropic displacement vectors of this intralayer H, however, no evidence for a second maximum was found. The diffraction patterns show diffuse scattering in streaks parallel to  $[001]^*$  through  $hkl$  reflections with  $hk \neq 0$ , which is caused by stacking faults. No twinning was observed for either of the two crystals.

**Key Words**—Crystal Structure, Diffuse Scattering, H-Positions, Kaolinite, Microcrystal, Single Crystal Refinement, Synchrotron Radiation.

### INTRODUCTION

Kaolinite crystals from geodes found near Keokuk, Iowa, are often of exceptional quality. Samples do not generally show asymmetric line broadening in powder X-ray and neutron diffraction patterns, and this indicates a lack of stacking faults. Kaolinite from Keokuk was a focus of several studies with conflicting results. Adams (1983), Bish and Von Dreele (1989), Smrčok *et al.* (1990), and Bish (1993) described the structure refined from X-ray and neutron powder data in space group  $C1$ . Suitch and Young (1983) and Young and Hewat (1988) refined the structure from X-ray and neutron powder data in space group  $P1$ . Both groups agreed on the position of all but one OH group. By considering the lower symmetry, Suitch and Young (1983) and Young and Hewat (1988) found two different orientations for the intralayer OH group, one pointing toward and one away from the octahedral sheet. This interpretation of different OH orientations was questioned by the other authors. Bish and Von Dreele (1989) and Smrčok *et al.* (1990) noted that some of the Si-O bond lengths in the refinement by Suitch and Young (1983) are outside the range usually found in silicates, indicating errors with the refinement. Bish and Von Dreele (1989) showed that kaolinite from Keokuk contains small amounts of dickite, which were not considered by Suitch and Young (1983). Thompson and Withers (1987) and Thompson

*et al.* (1989) did not find reflections in violation of  $C$ -centering in electron diffraction patterns. Young and Hewat (1988) noted, however, that the difference between the two hydrogen positions is related to variations in the  $z$  parameter and might not be observable by electron diffraction.

Recently, Hobbs *et al.* (1997) modeled the kaolinite structure by an all-atom *ab initio* energy minimization method. Their results confirm space group  $C1$  as well. Their calculations predict significantly different Si-O bond lengths for the basal and the apical oxygen atoms, which were not observed by Bish and Von Dreele (1989) and Bish (1993).

Single crystals of kaolinite sufficiently large for standard single crystal work do not exist, although a few specimens to 1 mm in thickness are known. These are, however, not true single crystals but rather stacks of crystals in very similar orientation. The quality is not sufficient for structure refinement. Recent advances in synchrotron radiation, notably at the microfocus beam line ID13 at the European Synchrotron Radiation Facility (ESRF), allow single-crystal diffraction experiments on micrometer and submicrometer-sized crystals.

This study presents an additional proof of the space group based on single crystal data and demonstrates the ability of micro-crystal diffraction techniques at a third generation synchrotron source.

### SAMPLE PREPARATION

The crystals used for this study are from Keokuk, Iowa. The largest crystals are platy with diameters of  $\sim 5 \mu\text{m}$  and a thickness of  $< 1 \mu\text{m}$ . Most of the crystals are much smaller.

<sup>†</sup> Present address: Mineralogisches Institut, Am Hubland, 97074 Würzburg, Germany.

<sup>‡</sup> Present address: ESRF, B.P. Box 220, 38043 Grenoble, France.

<sup>§</sup> Present address: Siemens AG.

Table 1. Experimental parameters.

Crystal	8 $\mu\text{m}^3$	0.8 $\mu\text{m}^3$
Wavelength	0.6883	0.6883
T <sub>measurement</sub>	293 K	293 K
2 $\theta_{\text{max}}$	77.09°	76.67°
N(hkl) <sub>observed</sub>	2777	3283
N(hkl) <sub>unique</sub>	2433	2404
R <sub>int</sub>	0.0250	0.0457
N(parameter) <sub>refined</sub>	128	125
R <sub>w</sub> (F <sup>2</sup> ) <sup>1</sup>	0.0929	0.167
R(F) > 4 $\sigma$ <sup>2</sup>	0.035	0.059
R(F) <sub>all data</sub> <sup>3</sup>	0.044	0.074

<sup>1</sup> Weighted residual based on  $F^2$ :  $R_w(F^2) = \{ \sum [\omega(F_o^2 - F_c^2)^2] / \sum [\omega(F_o^2)^2] \}^{1/2}$ .

<sup>2</sup> Residual based on  $F$  for reflections with  $F_o^2$  larger than  $4\sigma$ :  $R(F) = \{ \sum \|F_o\| - |F_c| / \sum |F_o\| \}$ .

<sup>3</sup> Residual based on  $F$  for all reflections.

Crystals of these dimensions are too small for the application of standard mounting techniques used for single-crystal work. The resolution of optical microscopes with an inverse light path used for microcrystal preparation is limited to samples of  $>5 \mu\text{m}$  in diameter.

Recently, we demonstrated a novel mounting technique for individual single crystals of  $<1 \mu\text{m}$  in diameter (Neder *et al.*, 1996a). The crystals are glued to a submicrometer glass fiber in a scanning electron microscope (SEM). Glass fibers are ideal sample supports for microcrystal diffraction experiments due to negligible scattering. Such fibers are specially prepared to a diameter of  $\sim 0.5\text{--}1 \mu\text{m}$  by using a microforge. A Zeiss SEM DSM 960 was used to mount the crystal on the fiber. The large sample chamber ( $30 \times 30 \times 30 \text{ cm}$ ) of this SEM offers sufficient space for the micromanipulator. This micromanipulator consists of three stepper-motor-driven mechanical translation units, each equipped with an additional piezoelectric drive. The travel range of the translation units is  $5 \text{ mm}$  at a resolution of  $\sim 50 \text{ nm}$ .

Kaolinite powder was carefully dispersed by a small blast of pressurized air and allowed to sediment in air onto a polished copper disk. No coating by carbon or gold was applied prior to the observation of the crystals in the SEM. Although a C or Au coating will improve the quality of the SEM image, a coating will produce a powder pattern that renders the proper integration of microcrystal X-ray reflection data impossible. A set of suitable crystals was selected on the basis of their size and shape. The glass fiber was covered with a very small drop of a two-component resin (XW 396/XW 397, manufactured by Ciba). This resin has a negligible vapor pressure and remains liquid sufficiently long under high-vacuum conditions until the fiber is brought into contact with the target crystal. Once the resin hardens, the crystal position is verified and the approximate thickness is measured. In the initial state of contact with the fluid resin, almost all

plate-like crystals move into a position with the normal to the plate perpendicular to the glass fiber. The contact area is small compared with the diameter of the crystals, and no strain is believed to exist due to the mounting technique.

Two crystals were used for the experiments, with dimensions of approximately  $2 \times 4 \times 1 \mu\text{m}$  and  $2 \times 2 \times 0.2 \mu\text{m}$ . Since the samples could not be coated and the imaging quality of the SEM was only fair, the thickness is an estimate.

## EXPERIMENTAL METHODS

The experiments were performed at beam line ID13, ESRF, Grenoble, France, at room temperature at a fixed wavelength of  $0.6883 \text{ \AA}$ . The wavelength was determined by an extended X-ray absorption fine structure (EXAFS) experiment at the Zr edge and is accurate to  $\sim 0.001 \text{ \AA}$ . This beamline uses an undulator beam that is monochromatized by a silicon 111 double monochromator and focused onto the sample by an ellipsoidally polished mirror. Data were collected by the oscillation technique, using a two-dimensional CCD detector (Koch, 1994) and with the fiber axis approximately parallel to the oscillation axis. The oscillation range of each exposure was  $8^\circ$  with a  $3^\circ$  overlap between adjacent oscillations. A full  $360^\circ$  rotation was covered by the oscillations. Exposure time ranged from 10 to 750 s. To reduce the background, small primary collimators of 30 and  $10 \mu\text{m}$  diameter were placed at a distance of  $1 \text{ mm}$  to the sample, and a beam stop was positioned  $7 \text{ mm}$  behind the sample. The sample-detector distance was  $56.90 \text{ mm}$ . At this distance, the area detector collects data from an  $80^\circ$  cone. Data were collected with the center of the area detector at  $2\theta = 0^\circ$  and  $2\theta = 35^\circ$ , which yielded reflections to  $2\theta_{\text{max}} = 76^\circ$ , *i.e.*,  $\sin(\theta)/\lambda = 0.89$ . Both crystals were oriented with the [001] direction approximately normal to the rotation axis. The two crystals were rotated with respect to each other around the [001] direction by  $\sim 90^\circ$  and thus, the two data sets yielded complementary reflections. The data were corrected for spatial sensitivity fluctuations. No distortion correction is necessary for the CCD detector. The determination of the orientation matrix and the integration of reflections used the DENZO program at the ESRF. No absorption correction was made since the maximum absorption of the micro-crystals was  $<0.2\%$ . The unit-cell parameters are  $a = 5.154(9) \text{ \AA}$ ,  $b = 8.942(4) \text{ \AA}$ ,  $c = 7.401(10) \text{ \AA}$ ,  $\alpha = 91.69(9)^\circ$ ,  $\beta = 104.61(5)^\circ$ ,  $\gamma = 89.82(4)^\circ$ . Experimental parameters are listed in Table 1.

Integration showed no intensity at  $h + k \neq 2n$  positions, thus indicating C-centering and space group C1. The crystal structure of the non-hydrogen atoms was determined by direct methods using SHELX-97. The structure involving the non-hydrogen atoms is consistent with previously published kaolinite struc-

Table 2. Different H(1) models.

Parameters	$R_w(F^2)$	$x$	$y$	$z$	Occ <sup>1</sup>	U	Bond dist (Å)
H(1) omitted	0.0940						
xyz, occ, U	0.0926	0.128(15) <sup>1</sup>	0.039(11)	0.334(10)	0.49(11)	0.00(2)	0.74(9)
xyz, U	0.0925	0.252(29)	0.038(22)	0.371(23)	1.0	0.22(8)	1.18(16)
U	0.0929	0.1423	0.0353	0.3474	1.0	0.19(6)	0.748(3)

<sup>1</sup> Values in parentheses are estimated standard deviations as given in the last decimal place, Occ = site occupancy.

tures. After initial refinement with isotropic atomic displacement parameters, a full anisotropic refinement with independent parameters for all non-hydrogen atoms was completed. Difference-Fourier maps revealed the positions of the three interlayer and the intralayer H atoms. The positions and isotropic displacement parameters for the three interlayer H atoms were refined.

Refinement of the intralayer H was more difficult. When the position, occupancy parameter, and isotropic U are refined, the occupancy drops to 0.5(1) and the U value obtained is zero, which is not physically reasonable. Subsequent refinement cycles showed that the occupancy and the U(H1) are strongly correlated. A refinement of OH(1) occupancy resulted in full occupancy, and we fixed the occupancy at this value for further modeling. Simultaneous refinement of both the position and U of H(1) yielded a value of 1.18 Å for the O-H(1) bond distance, which is greater than the expected value of 0.88–0.92 Å for a refinement using X-ray data. For the final model, both the occupancy and the position of H(1) were fixed and only the U of H(1) was refined, which resulted in a value of 0.18(6) Å<sup>2</sup>. The weighted R-values, atomic parameters of H(1), and the O-H(1) bond length of these models are presented in Table 2.

The final model converged to a weighted R-value based on  $F^2$  of 0.0929, based on all 2433 reflections

and 128 parameters. Except for fixing the H(1) position, no part of the refinement or structure was constrained. Table 3 lists the final atomic parameters for Keokuk kaolinite and Table 4 lists the atomic displacement parameters.

#### DIFFUSE SCATTERING AND ANALYSIS OF TWINNING

Quite surprisingly for a crystal of as little as 8  $\mu\text{m}^3$  volume, the intensity at beamline ID13 was sufficient to record diffuse scattering. Note that the powder pattern of kaolinite from Keokuk shows little diffuse scattering. Diffraction patterns (Figure 1) show very weak diffuse streaks parallel to [001]\* through Bragg reflections, except for the 00 $l$  reflections, where the diffuse scattering is not observed. The intensity of the diffuse rods quickly decays with increasing distance from the Bragg reflection. Except for one weak spot along the streak from the 021 to the 022 reflection at  $l \sim 1.3$  the decrease of the intensities is not modulated. No diffuse scattering is observed in the  $hk0$  plane.

This one-dimensional diffuse scattering is explained by stacking faults. The absence of observable diffuse scattering through the 00 $l$  reflections shows that the stacking consists of identical 7-Å layers and that the stacking faults consist of shifts of layers in the (001) plane. Different types of layers or a variation in  $d$ -value between the layers is non-existent. The observed diffuse scattering was too weak to determine if reflections with  $k = 3n$  showed less diffuse scattering, as is commonly observed. A recent study of diffuse X-ray scattering by a kaolinite micro-crystal from Georgia (Grasl *et al.*, 1998) did reveal that the diffuse scattering through  $k = 3n$  reflections is weak compared to that through the other reflections. The intensity distribution of the diffuse scattering suggests that the stacking faults are distributed at random intervals in the crystal. This observation shows that the Keokuk kaolinite, a kaolinite of exceptional quality as expressed by the Hinckley index of 1.90, is slightly disordered. Although this effect is small, it may have contributed to the difficulties encountered in the powder refinements of Suitch and Young (1983) and Young and Hewat (1988). The diffuse scattering observed in this experiment was too weak, however, to be analyzed in further detail.

This diffuse scattering is, with one notable exception, consistent with stacking faults of the kaolinite

Table 3. Final atomic parameters for Keokuk kaolinite.

Atom	$x$	$y$	$z$
Al(1)	0.2986(4) <sup>1</sup>	0.4955(3)	0.4755(3)
Al(2)	0.7937(4)	0.3306(3)	0.4744(3)
Si(1)	-0.0032(4)	0.3383(3)	0.0924(3)
Si(2)	0.5108(4)	0.1668(3)	0.0938(3)
O(1)	0.0503(5)	0.3538(4)	0.3161(3)
O(2)	0.1217(5)	0.6627(4)	0.3166(4)
O(3)	0.0	0.5	0.0
O(4)	0.2103(5)	0.2318(4)	0.0244(3)
O(5)	0.2037(5)	0.7639(4)	0.0003(3)
OH(1)	0.0504(5)	0.9687(4)	0.3253(4)
OH(2)	-0.0411(5)	0.1657(4)	0.6043(4)
OH(3)	0.0373(5)	0.4732(4)	0.6041(4)
OH(4)	0.0364(5)	0.8564(4)	0.6080(4)
H(1)	0.14230	1.03530	0.34740
H(2)	0.056(11)	0.180(8)	0.701(9)
H(3)	0.036(15)	0.486(11)	0.708(12)
H(4)	0.033(11)	0.795(8)	0.698(8)

<sup>1</sup> Values in parentheses are estimated standard deviations as given in the last decimal place.



Table 4. Anisotropic displacement parameters.

Atom	$U_{11}$	$U_{22}$	$U_{33}$	$U_{23}$	$U_{13}$	$U_{12}$	$U_{eq}^1$
Al1	0.0077(3) <sup>2</sup>	0.0088(7)	0.0074(3)	-0.0004(3)	0.0016(2)	0.0001(3)	0.0080(2)
Al2	0.0078(3)	0.0088(7)	0.0082(4)	-0.0001(3)	0.0016(3)	0.0001(3)	0.0084(2)
Si1	0.0068(2)	0.0078(6)	0.0066(3)	-0.0003(3)	0.0018(2)	-0.0005(3)	0.0071(2)
Si2	0.0062(2)	0.0075(6)	0.0072(3)	-0.0001(3)	0.0017(2)	-0.0002(3)	0.0070(2)
O1	0.0072(6)	0.0117(15)	0.0065(6)	-0.0019(7)	0.0020(5)	-0.0014(6)	0.0085(4)
O2	0.0097(6)	0.0101(15)	0.0070(7)	-0.0003(7)	0.0006(5)	-0.0016(6)	0.0092(4)
O3	0.0142(7)	0.0093(15)	0.0104(7)	-0.0001(7)	0.0030(5)	0.0000(7)	0.0114(4)
O4	0.0074(6)	0.0132(16)	0.0112(7)	-0.0016(7)	0.0018(5)	0.0039(7)	0.0108(5)
O5	0.0081(6)	0.0124(15)	0.0086(7)	0.0010(7)	0.0020(5)	-0.0035(6)	0.0097(4)
OH1	0.0092(7)	0.0122(16)	0.0124(8)	0.0028(7)	0.0038(5)	0.0031(6)	0.0110(5)
OH2	0.0116(7)	0.0097(16)	0.0095(7)	0.0002(7)	-0.0016(6)	0.0001(7)	0.0110(5)
OH3	0.0112(7)	0.0131(16)	0.0094(7)	-0.0048(8)	0.0047(6)	-0.0032(7)	0.0110(5)
OH4	0.0108(7)	0.0151(18)	0.0094(7)	0.0026(8)	0.0034(6)	0.0021(7)	0.0116(5)
H1							0.194(58)
H2							0.034(15)
H3							0.082(28)
H4							0.028(13)

<sup>1</sup> For non-hydrogen atoms equivalent isotropic U, for hydrogen atoms isotropic U.

<sup>2</sup> Values in parentheses are estimated standard deviations as given in the last decimal place.

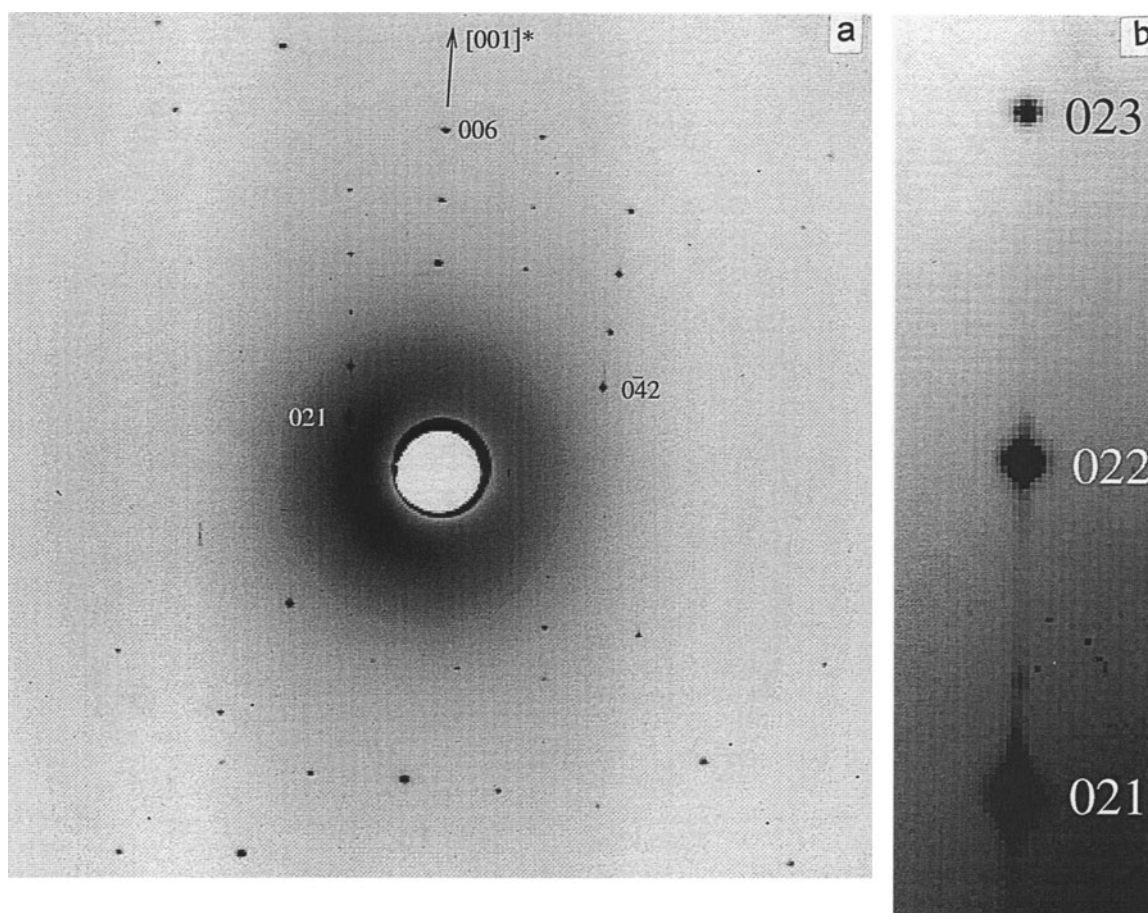


Figure 1. Section of the diffraction pattern of the 8  $\mu\text{m}^3$  crystal. (a) The enlarged section shows the diffuse scattering parallel to  $[001]^*$  through the  $02l$  reflections. (b) The reflection at the bottom of this enlargement is the 021.

Table 5. Si-O and Al-O bond lengths (Å) for kaolinite.

Bond	Distance (Å)	Bond	Distance (Å)
Si(1)-O(1)	1.614(3) <sup>1</sup>	Si(2)-O(2)	1.605(3)
-O(3)	1.620(3)	-O(3)	1.622(3)
-O(4)	1.618(3)	-O(4)	1.616(3)
-O(5)	1.628(3)	-O(5)	1.615(3)
Al(1)-O(1)	1.948(3)	Al(2)-O(1)	1.990(3)
-O(2)	2.001(3)	-O(2)	1.946(3)
-OH(1)	1.921(3)	-OH(1)	1.921(3)
-OH(2)	1.853(3)	-OH(2)	1.867(3)
-OH(3)	1.849(3)	-OH(3)	1.858(3)
-OH(4)	1.862(3)	-OH(4)	1.853(3)

<sup>1</sup> Values in parentheses are estimated standard deviations as given in the last decimal place.

structure as reported by Bookin *et al.* (1989), Plançon *et al.* (1989), and references therein. Bookin *et al.* (1989) analyzed the stacking models previously proposed in the literature. Based on arguments related to the lattice constants and the relative location of Si and Al atoms in adjacent layers, the  $\pm b/3$ , the  $\pm 120^\circ$ , and the vacancy displacement models were rejected. Two models were proposed, one with identical layers shifted by [0.017, 0.328, 0.0] and a second consisting of right- and left-handed kaolinite. They proposed that a mirror plane is normal to the (001) plane along the trace of the [110] direction, and calculated powder diffraction patterns are shown for the two models that are nearly similar. Accordingly, Bookin *et al.* (1989) concluded that an experimental distinction is problematic.

This distinction is, however, possible in a single crystal experiment. A crystal containing only stacking faults between identical layers with a shift vector of [0.017, 0.328, 0.0] will display a diffraction pattern with rods of diffuse scattering along the [001]\* direction through all Bragg reflections, except the 00*l* reflections. If stacking faults occur at random intervals, the intensity will fade uniformly with increasing distance from the Bragg reflection. For a model with layers related by twinning, the diffraction pattern will differ. Kaolinite from Keokuk shows very weak diffuse scattering which means that the probability of stacking faults is low. A crystal with stacking faults involving layers related by twinning would consist of a few thick blocks of right- and left-handed kaolinite. Reciprocal space of such a crystal would consist of the overlay of the right- and left-handed reciprocal lattices. Due to the triclinic unit-cell shape, the Bragg reflections from the two twins will not coincide. The mirror plane suggested by Bookin *et al.* (1989) will transform the Bragg reflections of left-handed kaolinite to non-integer positions in the reciprocal space of right-handed kaolinite and *vice versa*. The  $1\bar{1}0$  Bragg reflection of left-handed kaolinite, for example, expressed in terms of the reciprocal lattice vectors of right-handed kaolinite is located at  $\bar{1}, 1, 0.6888$ , *i.e.*, at non-integer *l*. The diffuse rods will be strongly modulated and the nature

of the modulation depends on the probability of stacking faults. The observed diffraction patterns do not show these modulations. Hence, the observed diffuse scattering of this crystal is not related to stacking faults from twinning relationships but are due to shifted layers.

Since the shape of the unit cell of kaolinite is triclinic, merohedral twins can not exist. The only twinning relationship where Bragg reflections will superpose is a twin involving a center of inversion. Since this implies stacking where adjacent 1:1 layers have opposing tetrahedral sheets or opposing octahedral sheets across the interlayer, this type of twinning is energetically very implausible. Since all observed Bragg reflections can be indexed with a single orientation matrix, the present crystal is untwinned. Twinning due to a mirror plane normal to the (001) plane along the trace of the [110] direction, however, was observed in the diffraction pattern of another single crystal of 0.4  $\mu\text{m}^3$  volume by Neder *et al.* (1996b).

## RESULTS AND DISCUSSION

The experimental observations are clearly consistent with space group *C1*. No reflections violating the space group were observed. The structure refines well in this space group and the non-hydrogen structure is very similar to the room-temperature X-ray powder diffraction study of Bish and VonDreele (1989) and the low-temperature neutron powder diffraction study of Bish (1993). Bish (1993) noted that the temperature decrease mostly affects the interlayer separation. The structure of the tetrahedral and octahedral sheets are nearly identical, although the octahedral thickness is slightly smaller at low temperature.

The Si tetrahedra show a short Si-O<sub>apical</sub> distance and larger Si-O<sub>basal</sub> distances (Table 5), with the Si-O<sub>apical</sub> bond 0.013 Å shorter than the average Si-O<sub>basal</sub> bond. The corresponding bonds in the two tetrahedra are nearly identical. These results confirm the model of Hobbs *et al.* (1997), although the observed differences between the bond lengths are smaller than those reported by Hobbs *et al.* (1997). In contrast to the current results, the X-ray powder refinements of Bish and VonDreele (1989) yielded a longer Si-O<sub>apical</sub> bond distance for the Si(2) tetrahedron, whereas the distances in the Si(1) tetrahedron showed no systematic relationship. The low-temperature neutron powder diffraction study of Bish (1993) showed no bond length differences in either tetrahedron.

The Al-(O,OH) distances of this study are similar to those observed by Bish and VonDreele (1989) and Bish (1993) and calculated by Hobbs *et al.* (1997). The Al-O<sub>apical</sub> bonds are significantly longer than the Al-OH bonds and the Al-OH(1) bond to the intralayer hydroxyl group is longer than the Al-OH bonds to the interlayer hydroxyl groups. The two Al octahedra are nearly identical. The six Al-O bonds fall into two

Table 6. Structural parameters for OH groups in kaolinite.

Atom	O-H (Å)	Angle of OH with <i>b</i> axis <sup>1</sup>	Angle of OH with (001) plane	O-O Distance for H bond O-H...O(Å)	∠(DHA)
OH(1)	0.75	36°	12°		
OH(2)	0.76(6) <sup>2</sup>	72(5)°	64(4)°	..O(4) 3.088(3)	160(6)°
OH(3)	0.77(9)	64(5)°	73(10)°	..O(4) 2.989(3)	173(9)°
OH(4)	0.88(7)	162(5) <sup>3</sup>	47(5)°	..O(4) 2.953(3)	142(5)°

<sup>1</sup> For easier comparison with Bish (1993) this angle is the angle between the *b* axis and the projection of the OH vector along the normal to the (001) plane onto the (001) plane.

<sup>2</sup> Values in parentheses are estimated standard deviations as given in the last decimal place.

<sup>3</sup> Bish (1993) lists the angle to the negative *b* axis.

groups with bond lengths of ~1.85 and 1.94 Å, respectively. The oxygen atoms involved in the three longer bonds (two Al-O<sub>apical</sub> bonds, Al-OH(1) bond) form the oxygen atom plane that is common to both the octahedral and tetrahedral sheets. The fact that the Al-O<sub>apical</sub> bonds involve oxygen atoms that are shared by two Al octahedra and the Si tetrahedra, whereas the Al-OH(1) bond involves an oxygen atom that is shared by two Al octahedra only, appears to play only a minor role.

The bond lengths and bond angles within the two tetrahedra around Si(1) and Si(2) are very similar to each other, as is the connectivity of these polyhedra to the adjacent Si tetrahedra and Al octahedra. Consequently, the mean-square displacements of the two Si atoms are similar. Although Al octahedra display two groups of slightly different bond lengths, the respective bond lengths and bond angles within the two octahedra and their respective connectivity to adjacent octahedra are very similar. Thus the atomic displacement parameters of Al(1) and Al(2) are also similar. Both Si atoms show almost isotropic displacement parameters, because the Si occupies the center of an almost regular tetrahedron. Apparently, the differences between the potentials of the Si-O<sub>apical</sub> bonds and the Si-O<sub>basal</sub> bonds are too weak to induce anisotropic displacements. The Al octahedra deviate slightly from a regular polyhedron and the six oxygen neighbors are involved in different topologies. Since the observed deviation from isotropic displacements is small, the shape of the potential field distribution at the Al site must be nearly that of a regular octahedron. The oxygen atoms show more pronounced anisotropic displacement vectors since they are involved in more irregular coordination and the potential along the Si-O bond is expected to be very different from the potential in a plane normal to this bond.

The interlayer O-H vectors associated with the H bonding are nearly normal to the (001) plane (Table 6). The O-H bond distances are 0.76–0.88 Å, which

are acceptable values for X-ray data. The O-O distances for O-H...O are 2.953(3), 2.989(3), and 3.088(3) Å, with bond angles of 142(5)°, 173(9)°, and 160(6)° at the vertex of the H atom.

#### Position of the intralayer hydrogen

As noted above, the position of the intralayer hydrogen could not be refined, although its location was determined by difference-Fourier methods. Two cross sections through the difference map (Figure 2) show one maximum at 0.142, 0.035, 0.347. No evidence exists for a second maximum either above or below the *z* = 0.347 plane, as would be expected if the space group *P1* (Young and Hewat, 1988) is correct. Besides the systematic absences of *h* + *k* ≠ 2*n*, this is further evidence for space group *C1*.

The displacement parameter of H(1) is large for normal thermal vibrations. Considering the constraints applied during the refinement, the magnitude of the displacement parameter must be interpreted with caution. However, the distribution of electron density in the difference-Fourier maps is consistent with the large value of the displacement parameter. These difference-Fourier maps (Figure 2) show electron density near the H(1) position [as calculated from a model without H(1)]. The density distribution is clearly anisotropic and approximately arc shaped, which suggests a thermal libration of the H(1) position around the corresponding OH(1) position at a nearly constant bond distance. The corresponding difference-Fourier maps of the interlayer H atoms do not show such delocalized and anisotropic electron densities. Such a density distribution cannot be described by an isotropic atomic displacement parameter. Contrary to the low-temperature neutron powder diffraction study (Bish, 1993), the shape of the difference-Fourier peak shows its greatest elongation in the (001) plane. The current results, however, were obtained from single-crystal X-ray data collected at room temperature, which are less reliable for determining the location of hydrogen atoms than neutron experiments.

A more detailed analysis of anisotropic displacement parameters for H(1) is not possible because the scattering amplitude of hydrogen is too small. The high value of *U*(H1) probably results from both thermal vibration and random static displacement. These observations are in agreement with those of Bish (1993). The angle between the O-H(1) bond and the (001) plane is 12° (Table 6) and, based on the difference map, the estimated standard deviation is near 5°. Thus, the observed angle of 12(5)° is higher than the angle (0.34°) observed by Bish (1993) or that calculated (3.8°) by Hobbs *et al.* (1997) and reported (3.8°) by Hess and Saunders (1992). However, large temperature differences between the experimental conditions makes comparison difficult.



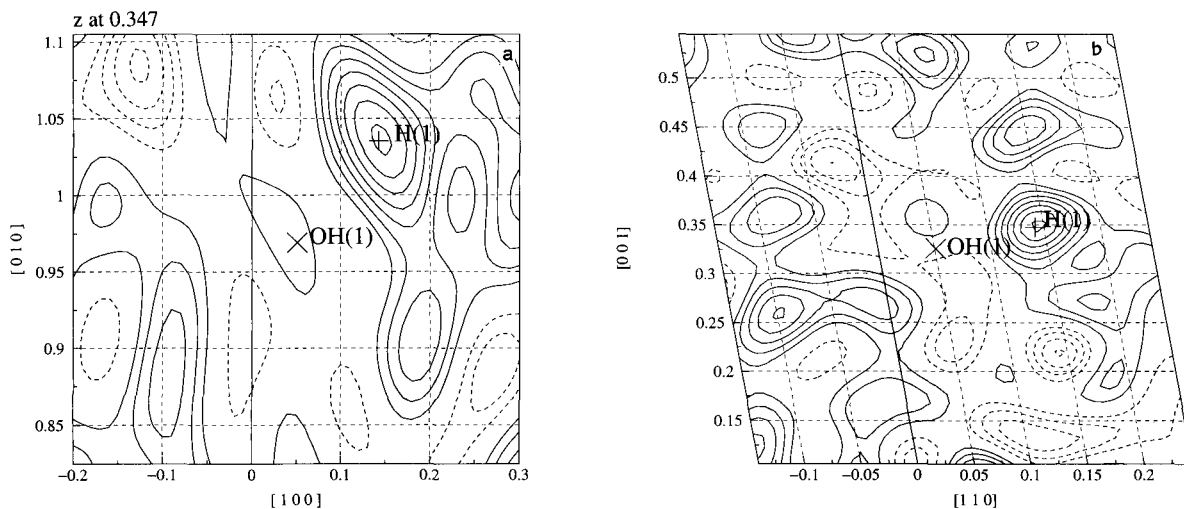


Figure 2. Difference-Fourier map of the final model without H(1) included in the model. The contour lines are in intervals of 0.1 electrons/Å<sup>3</sup>, starting at 0.1 and -0.1, respectively. a) Difference-Fourier map in the (001) plane at the  $z$  of the maximum difference-Fourier at  $z = 0.347$ . The (×) in the center of the plot corresponds to the final refined  $x,y$  position of the OH(1), which is at  $z = 0.325$ , and the (+) corresponds to the  $x,y$  position of H(1). b) Difference-Fourier map in the plane defined by the OH-vector and the  $c$  axis. This plane is at an angle of 7° to the (110) plane. The (×) in the center of the plot corresponds to the final refined  $x,z$  position of OH(1), and the (+) corresponds to the  $x,z$  position of H(1).

Also, energy-minimization calculations are strictly valid at  $T = 0$  K.

As expected from a refinement based on X-ray data, the positional parameters of the H atoms are of lower precision than the non-hydrogen atoms. However, for a crystal of volume of only 8 μm<sup>3</sup>, the refinement of the H positions and their isotropic displacement parameters are quite remarkable. Such results were obtained because of the high signal-to-noise ratio and the numerous high-angle reflections ( $2\theta_{max} = 76^\circ$ ) processed.

#### ACKNOWLEDGMENTS

We are indebted to W. Keller, University of Missouri, who kindly supplied the kaolinite samples from Keokuk, Iowa. We appreciate the support by H. Koop, Institute for Botany, University München, who showed us how to make the micrometer-sized glass fibers. The samples were mounted, using the SEM at the Department of Geosciences, University of München. A travel grant and beam time at the ESRF is gratefully acknowledged. This work was supported by the BMBF under grant 05 647 WMA5. We are especially thankful for the constructive criticism of the reviewers.

#### REFERENCES

- Adams, J.M. (1983) Hydrogen atom positions in kaolinite by neutron profile refinement. *Clays and Clay Minerals*, **31**, 352–356.
- Bish, D.L. (1993) Rietveld refinement of the kaolinite structure at 1.5 K. *Clays and Clay Minerals*, **41**, 738–744.
- Bish, D.L. and Von Dreele, R.B. (1989) Rietveld refinement of non-hydrogen atom positions in kaolinite. *Clays and Clay Minerals*, **37**, 289–296.
- Bookin, A.S., Drits, V.A., Plançon, A., and Tschoubar, C. (1989) Stacking faults in kaolinite-group minerals in the light of real structural features. *Clays and Clay Minerals*, **37**, 297–307.
- Grasl, T., Neder, R.B., Schulz, H., and Burghammer, M. (1998) Einkristallbeugungsexperimente an einem stark fehlgeordneten Kaolinit. *Zeitschrift für Kristallographie, Supplement*, **15**, 136.
- Hess, A.C. and Saunders, V.R. (1992) Periodic ab initio Hartree-Fock calculations of the low-symmetry mineral Kaolinite. *The Journal of Physical Chemistry*, **96**, 4367–4374.
- Hobbs, J.D., Cygan, R.T., Nagy, K.L., Schultz, P.A., and Sears, M.P. (1997) All-atom ab initio energy minimization of the kaolinite crystal structure. *American Mineralogist*, **82**, 657–662.
- Koch, A. (1994) Lens coupled scintillating screen-CCD X-ray area detector with a high detective quantum efficiency. *Nuclear Instruments and Methods in Physics Research A*, **348**, 654–658.
- Neder, R.B., Burghammer, M., Grasl, T., and Schulz, H. (1996a) Mounting an individual submicrometer sized crystal. *Zeitschrift für Kristallographie*, **211**, 365–367.
- Neder, R.B., Burghammer, M., Grasl, T., Schulz, H., Bram, A., Fiedler, S., and Riekel, Ch. (1996b) Single crystal diffraction by submicrometer sized kaolinite: observation of Bragg reflections and diffuse scattering. *Zeitschrift für Kristallographie*, **211**, 763–765.
- Plançon, A., Giese, R.F., Snyder, R., Drits, V.A., and Bookin, A.S. (1989) Stacking faults in the kaolinite-group minerals: Defect structures of kaolinite. *Clays and Clay Minerals*, **37**, 203–210.
- Smrčok, L., Gyepesová, D., and Chmielová, M. (1990) New X-ray Rietveld refinement of kaolinite from Keokuk, Iowa. *Crystal Research and Technology*, **25**, 105–110.
- Suitch, P.R. and Young, R.A. (1983) Atom positions in highly ordered kaolinite. *Clays and Clay Minerals*, **31**, 357–366.

- Thompson, J.G. and Withers, R.L. (1987) A transmission electron microscopy contribution to the structure of kaolinite. *Clays and Clay Minerals*, **35**, 237–239.
- Thompson, J.G., Fitz Gerald, J.D., and Withers, R.L. (1989) Electron diffraction evidence for C-centering of non-hydrogen atoms in kaolinite. *Clays and Clay Minerals*, **37**, 563–565.
- Young, R.A. and Hewat, A.W. (1988) Verification of the triclinic crystal structure of kaolinite. *Clays and Clay Minerals*, **36**, 225–232.

(Received 2 April 1998; accepted 17 February 1999; Ms. 98-043)